Efficient adsorption of tetracycline in water by Mn and Ce co-doped MIL-100 composite oxide

Shuguang Zhu[a], Pengyu Zhang[a], Jie Zhang[a], Xiaojie Song[b], Yun Wang[a], Xiangxiang Wang[a], Jinyun Liu[c], Bai Sun[a],*

[a]*Anhui Advanced Technology Research Institute of Green Building, College of Environment and Energy Engineering, Anhui Jianzhu University, Hefei 230601, China, Tel. +86-551-63828252; Fax: +86-551-63828252; emails: bsun@mail.ustc.edu.cn (B. Sun), zhushuguang@ahjzu.edu.cn (S. Zhu), zpy110817@163.com (P. Zhang), 1045441563@qq.com (J. Zhang), 596820989@qq.com (Y. Wang), 350992818@qq.com (X. Wang)*
[b]*School of Materials and Chemical Engineering, Anhui Jianzhu University, Hefei 230601, China, email: 17433503@qq.com (X. Song)*
[c]*Key Laboratory of Functional Molecular Solids, Ministry of Education, College of Chemistry and Materials Science, Anhui Normal University, Wuhu 241002, China, email: jyliu@ahnu.edu.cn (J. Liu)*

ABSTRACT

In this study, a manganese cerium co-doped iron-based metal–organic frameworks composite oxide nanomaterial (MnCe/MIL-100) was prepared by solvothermal method and used to adsorb tetracycline (TC) from water. Scanning electron microscope, energy dispersive spectroscopy (EDS), X-ray diffraction were used to study the micro morphology, main element composition and crystal structure of the adsorbent. The experimental results were fitted by adsorption kinetics, adsorption isotherms and other models. In addition, the influence of the dosage of adsorbent and the pH of the solution on the adsorption performance and the reusability of the composite were also studied. It was found that the adsorption rate of MnCe/MIL-100 to TC can be as high as 100%. The adsorption kinetics of TC on MnCe/MIL-100 can be well described by pseudo-second-order model. At room temperature, the adsorption capacity is up to 210.971 mg/g, which is consistent with Langmuir isotherm. Through thermodynamic analysis, it is found that this process has the characteristic of absorbing heat, and this absorption is spontaneous. Meanwhile, MnCe/MIL-100 still has good TC adsorption capacity after five cycles, showing good reusability, which is of great significance to cost saving and environmental pollution reduction. Finally, the analysis by Fourier-transform infrared spectroscopy and zeta potential explain the mechanism of TC adsorption.

Keywords: Tetracycline; Adsorbent; Nanometer material; MnCe/MIL-100

1. Introduction

In recent years, antibiotics have been widely used in animal husbandry, aquaculture, human medical care and other industries, followed by the abuse of antibiotics and the release of antibiotics into the environment without treatment, resulting in the deterioration of the ecological environment and threatening human health [1,2]. Tetracycline (TC) is a broad-spectrum antibiotic produced by Streptomyces, which has a good sterilization effect by inhibiting the synthesis of bacterial proteins, so it is very common in daily production and use. TC is poorly absorbed and metabolized in the body, and is usually discharged into the ecological environment along with excreta [3]. The presence of TC has been detected in pharmaceutical wastewater, animal husbandry wastewater and hospital wastewater [4–6].

* Corresponding author.

At present, the common antibiotic wastewater treatment methods are mainly membrane separation method [7], advanced oxidation method [8–10], coagulation method [11], biological method [12] and adsorption method [13]. Compared with other treatments, adsorption is a non-destructive physical method, which is widely used in wastewater treatment because of its high efficiency and low cost. However, how to find a low-cost, high-efficiency and recyclable adsorbent has become a problem attracting researchers' attention. With the research of nanomaterials, nanomaterials have been proved to be good adsorbents due to their unique morphology and structural characteristics, and can be widely used to remove antibiotic from water. Liu et al. [14] prepared a kind of MoS_2@zeolite-5 nano material by combining ultrasonic and hydrothermal methods. It has good adsorption performance for tetracycline, and the pseudo-second-order kinetic model fits the adsorption process well. Tao et al. [15] prepared cellulose nanocrystal/graphene oxide complexes with three-dimensional structure for the removal of levofloxacin hydrochloride in water by adsorption. When the optimal pH value was 4, the removal rate was more than 80.1%, and the adsorption dose was 1.0 g/L. Song et al. [16] prepared MnO_2/graphene nanocomposite, which has good water solubility and the removal rate of TC is 99.4%. Hao et al. [17] prepared nanocomposites of zero by pyrolysis of agricultural waste lignocellulose hazelnut shell iron@ biochar at 298 K, pH 6–7, and contact time of 40 min, the adsorption amounts of oxytetracycline, chlortetracycline and TC were 52.7, 42.5 and 39.1 mg/g, respectively.

Metal cations such as Fe(III) and Mn(II) have high affinity to tetracycline, so metal oxides have potential as adsorbent [18]. Multi metal oxide nanomaterials overcome the limitations of single metal oxide nanomaterials in water treatment technology and become better adsorption materials. A Mg/Fe layered bimetallic hydroxide synthesized by Qiu et al. [19] was first used to adsorb low concentration norfloxacin antibiotics in water. The results showed that LDH adsorbent with Mg/Fe molar ratio of 5:1 exhibited excellent adsorption performance for removing norfloxacin at low concentration (20 mg/L). The adsorption capacity can reach 97.07 mg/g. Yu et al. [20] studied the SDZ removal ability of Fe/Mn binary oxides and compared it with that of iron hydroxide and manganese dioxide. In neutral solution, the maximum adsorption capacity of FMBO is much larger than that of the other two adsorbents, and fmbo is least affected by pH. The Mn doped Cu oxide was synthesized by Wu [21]. Due to the surface complexation of MODCO, it can effectively adsorb and remove tetracycline, oxytetracycline and chlortetracycline. Among metal oxide, manganese oxide has been widely used because of its high activity due to the instability of lattice oxygen and the ability to store oxygen in the crystal structure. Cerium as the most abundant rare earth element, Cerium oxide has broad application prospects in adsorption and catalysis due to its stable physical and chemical properties and its unique 4f electron layer structure. The combination of manganese and cerium can have good redox performance, and gradually enter the field of vision of researchers by enhancing the mobility of oxygen and improving its adsorption and catalytic activity. In addition, mixing Ce with low-cost metal (Fe)

may be beneficial to increase the adsorption capacity, and improve the separation of adsorbent and avoid the toxicity of Ce through magnetism. In recent years, metal–organic frameworks (MOFs) has been widely used as heterogeneous catalyst for pollutant degradation due to its various manufacturing methods, adjustable structures and various catalytic sites [22]. In addition, studies have shown that MOFs prepared by coordination of metal ions and organic ligands are mostly crystalline porous materials, which have great application value in the field of water pollution adsorption due to their advantages such as large specific surface area, rich pore structure, and a large number of unsaturated metal sites that can adsorb pollutants. MOFs materials centered on iron have been proved to have good adsorption performance due to their non-toxic and harmless, green and environmental protection, low cost, stable chemical properties, and high specific surface area and pore volume. Ma et al. [23] synthesized three iron-based MOFs materials, MIL-100(Fe), MIL-101(Fe) and MIL-53(Fe), and applied them to the adsorption of typical volatile organic compounds toluene. The adsorption performance was evaluated by static adsorption, dynamic penetration curve and adsorption kinetics. The results showed that MIL-100(Fe) had good adsorption for toluene. Li et al. [24] prepared R-MIL-100(Fe) by a new method of synthesizing MIL-100(Fe) at room temperature with organic amine as protonation agent, and had good adsorption performance for fluorine in water, with the maximum fluoride adsorption capacity of 23.53 mg/g. A zif-67 derived hollow cobalt sulfide hollow Co_3S_4 prepared by Liang [25] et al. has good adsorptivity to ciprofloxacin in water due to electrostatic interaction.

In this study, manganese cerium co-doped iron-based MOFs composite nanomaterials (MnCe/MIL-100) were prepared by simple solvothermal method and used as adsorbent for TC removal. Through a simple preparation method, Mn and Ce are co-doped into MIL-100 (Fe), which not only retains the advantages of MOFs as adsorbent, but also enables the adsorbent to obtain higher adsorption capacity through metal doping [26], thus showing excellent removal capacity of TC in water. It is necessary and significant to obtain adsorbent with high adsorption capacity for the removal of pollutants in the water environment. The adsorption performance and mechanism of MnCe/MIL-100 for TC has not been reported yet. In this work, the effects of adsorbent dosage, solution pH and adsorbent regeneration on the adsorption performance of TC were studied. The adsorption characteristics of TC removal were analyzed by adsorption kinetics, isotherms and thermodynamic models. Scanning electron microscope (SEM), X-ray diffraction (XRD) and EDS were used to study the micro morphology and main element composition of the adsorbent. The adsorption mechanism was analyzed by Fourier-transform infrared spectroscopy (FT-IR) and zeta potential.

2. Materials and methods

2.1. Reagents and instruments

The reagents used in the experiment mainly include $Ce(NO_3)_3 \cdot 6H_2O$ (99.5%), $FeCl_3 \cdot 6H_2O$ (99.0%) were purchased from Sinopharm Chemical Reagent Co., Ltd., (Shanghai,

China) without further purification. Pyromellitic acid ($C_9H_6O_6$, 98.0%), polyvinylpyrrolidone ((C_6H_9NO)$_n$) analytical purity, Macklin Biochemical Co., Ltd., (Shanghai, China) N,N-dimethylformamide ($HCON(CH_3)_2$, 99.5%), analytical purity, Damao Chemical Reagent Co., Ltd., (Tianjin, China). Anhydrous ethanol (99.7%), analytical purity, Xilong Scientific Co., Ltd., (Guangdong, China). $Mn(CH_3COO)_2 \cdot 4H_2O$ (98.0%), analytical purity, Tianjin Guangfu Fine Chemical Research Institute (Tianjin, China). Deionized water is prepared by FST-TOP-A24 super pure water equipment by Shanghai Fushite Instrument Equipment Co., Ltd., (Shanghai, China).

The instruments used in the experiment mainly include: DHG-9023A air drying box, Shanghai Yiheng Scientific Instrument Co., Ltd., (Shanghai, China). PHS-3C digital pH meter, Shanghai Yidian Scientific Instrument Co., Ltd., (Shanghai, China). PTFE reaction kettle, Shanghai Jinghong Experimental Equipment Co., Ltd., (Shanghai, China). FA2204N electronic balance, Shanghai Jinghai instrument Co., Ltd., (Shanghai, China). TG16K-II Table high-speed centrifuge, Shanghai ZhaoDi Biotechnology Co., Ltd., (Shanghai, China).

2.2. Fabrication of adsorbent

MnCe/MIL-100 was prepared by solvothermal technology. The preparation process was as follows: $FeCl_3 \cdot 6H_2O$ (0.270 g, 1 mM) and $C_9H_6O_6$ (0.210 g, 1 mM) were added to 20 mL of $HCON(CH_3)_2$ (DMF). The mixture solution was then sonicated for 10 min and placed in a 100 mL reaction kettle and heated in an oven at 150°C for 6 h. After cooling, the prepared sample was repeatedly washed with DMF and ethanol, and then dried at 60°C to prepare MIL-100(Fe) sample [27]. Then, a certain amount of MIL-100 (Fe), $Mn(CH_3COO)_2 \cdot 4H_2O$, $Ce(NO_3)_3 \cdot 6H_2O$ and (C_6H_9NO)$_n$ were added to the mixed solution of 12 mL water and 3 mL ethanol. The mixture was then refluxed at 90°C and held at this temperature for 3 h. After washing with ethanol for several times and drying in an oven at 60°C for 4 h, the final sample MnCe/MIL-100 was obtained.

2.3. Characterization

The surface morphology and structure of MnCe/MIL-100 were characterized by field emission scanning electron microscopy (SEM, AURIGA, ZEISS Company, Germany) coupled with an energy dispersive spectrometer (EDS, INCA X-Max 50, ZEISS Company, Germany). The X-ray diffractometer (XRD, PANalytical, Netherlands) with a Cu Kα source was used to analyze the crystalline structure. Fourier-transform infrared spectroscopy (FT-IR, Nexus-870, Thermo Nicolet, USA) was used to determine the change of surface properties. The zeta potentials of the adsorbent before and after adsorption were analyzed on a zetasizer nano zeta potential analyzer (Zeta potential analyzer, Zetasizer Nano Series, Malvern Instruments Ltd., Britain).

2.4. Batch adsorption experiments

2.4.1. Preparation of TC standard solution

50 mg of TC was dissolved in 100 mL of deionized water, sonicated for 10 min, and transferred to a 500 mL volumetric flask to complete constant volume, that is, 100 mg/L of TC standard solution. TC solution in all adsorption experiments was obtained by diluting the standard solution with deionized water. Prepared TC solution with concentration gradient of 5, 10, 20, 30, 40, 50 and 60 mg/L, and measured its absorbance at 357 nm wavelength by ultraviolet spectrophotometer (UV-2600i). Then the TC standard curve was obtained by linear regression analysis of the concentration and absorbance of tetracycline.

2.4.2. Calculation of adsorption capacity and removal rate

The adsorption capacity and removal rate are calculated by Eqs. (1) and (2) to measure the adsorption performance of the adsorbent [14,28].

$$q_e = \frac{(C_0 - C_e) \times V}{m} \tag{1}$$

$$\eta = \frac{(C_0 - C_e)}{m} \times 100\% \tag{2}$$

where C_o (mg/L) and C_e (mg/L) are the initial concentration before adding the adsorbent and the equilibrium concentration after adding the adsorbent, respectively; q_e (mg/g) is the adsorption capacity at the adsorption equilibrium; V (L) is the volume of TC solution; m (g) is the dosage of adsorbent; η is the removal rate of the adsorbent.

2.4.3. Effect of adsorbent dosage

5, 10, 15, 20, 25 and 30 mg of adsorbents were added to 100 mL of TC solution with a concentration of 10 mg/L, respectively. Then, shaking them for 18 h under shading. Taking samples for measurement to explore the effect of the amount of adsorbent on the adsorption performance.

2.4.4. Effect of pH

0.1 mol/L HCl and 1 mol/L NaOH solution were used to adjust the pH value of 100 mL TC solution with a concentration of 10 mg/L. The pH value range of the solution was set to 3–12. Then, 15 mg of adsorbent was added respectively, and the effect of pH on the adsorption performance was investigated by shading and shaking for 18 h.

2.4.5. Study on adsorption isotherms

In the study of adsorption isotherm of MnCe/MIL-100 on TC, take 100 mL of TC solution with concentration of 10, 20, 30, 40, 50, 60, 70 and 80 mg/L, 15 mg of MnCe/MIL-100 was added to it respectively, and then put 250 mL conical flask filled with TC solution and adsorbent into a constant temperature shaker for shading and shaking for 18 h (25°C, 160 rpm). After the end of oscillation, conduct high-speed centrifugation, take an appropriate amount of supernatant, and pass through 0.22 μM inorganic filter membrane, and the absorbance value was measured by UV-Vis.

2.4.6. Study on adsorption kinetics

In the study of adsorption kinetics, 15 mg of adsorbent was added to 100 mL of TC solution with a concentration of 10 mg/L, and the solution was shielded from light and stirred. First, take samples at 5, 30, 60 and 120 min respectively, and then take samples at an interval of 1 h until 1,200 min later.

2.4.7. Study on adsorption thermodynamics

In the study of adsorption thermodynamics, at 298, 308 and 318 K, respectively, the vibration frequency of 160 rpm was oscillated in a constant temperature shaker for 18 h. After the oscillation, centrifuge and filter, measure the absorbance value of TC solution at the absorption wavelength of 357 nm, and finally analyze the data to obtain the entropy change, enthalpy change and Gibbs free energy change of the adsorption experiment.

2.4.8. Study on regeneration capacity of adsorbent

In order to evaluate the regeneration ability of the adsorbent, pour a certain amount of saturated adsorbent into 0.1 mol/L NaOH solution for desorption and reuse. Repeat the five cycle regeneration experiments to explore the regeneration performance of MnCe/MIL-100.

3. Results and discussion

3.1. Sample characterization

Fig. 1a–d are SEM images of MnCe/MIL-100 before and after adsorption of TC, describing the changes of surface morphology before and after adsorption of TC by adsorbent. It can be seen from Fig. 1a and b that MnCe/MIL-100 sample presents a large number of regular ultrafine particles and some small rod-shaped structures. The particle structure may be manganese oxide or its solid solution with cerium oxide, while the rod structure is attributed to the aggregation of cerium oxide. In addition, abundant pore structures between the particles can be observed, which contributes to the adsorption of the adsorbent. Fig. 1c and d show the morphology and structure of MnCe/MIL-100 after adsorption. It can be seen that the spherical particles become fuller and the aggregates are obvious. This is because TC is adsorbed on the gap and surface of the adsorbent, which indicates that the material has an adsorption effect on TC [29].

In order to investigate the elemental composition and content of MnCe/MIL-100, the adsorbent was characterized by EDS. Table 1 lists the contents of various elements before and after adsorption, of which the oxygen element content accounts for the largest proportion, which indicates that there are a large number of oxygen-containing functional groups in MnCe/MIL-100. In addition, it can be seen from the table that the composite material contains a certain amount of manganese, iron and cerium, while nitrogen comes from MIL-100 MOFs, and silicon may come from the detection environment. After adsorption of TC, the relative content of C, N, O on the material surface increases, while the relative content of metal elements decreases, indicating that TC is adsorbed on the material surface.

The crystal structure of the prepared MnCe/MIL-100 was characterized, and the XRD pattern is shown in Fig. 2. In 2θ the diffraction peaks at 24.15°, 33.16°, 40.86°, 49.46°, 54.07°, 62.44° and 64.00° correspond to (012), (104), (113),
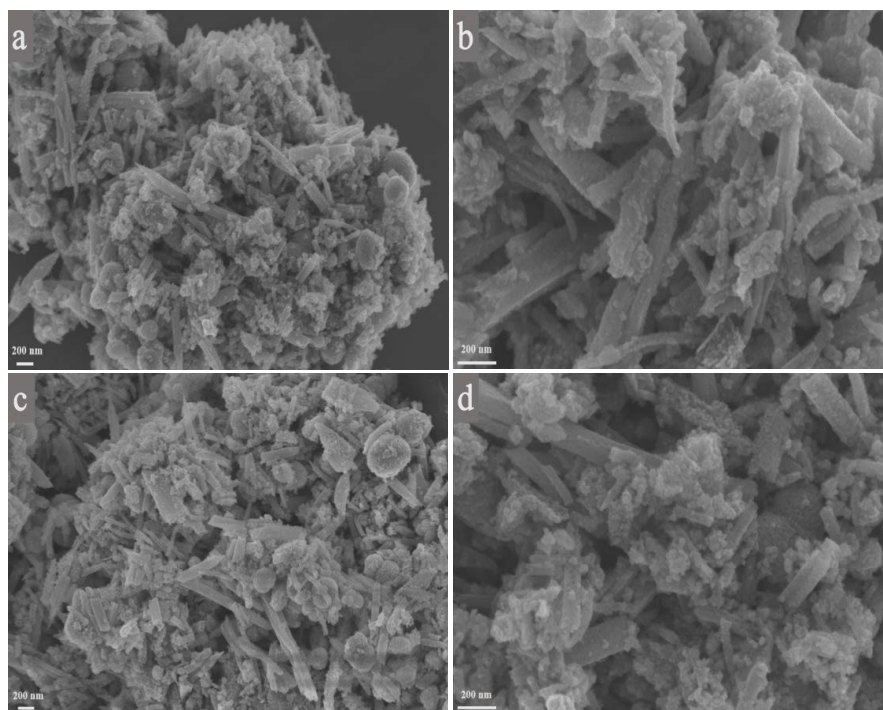
Fig. 1. (a, b) SEM images before MnCe/MIL-100 adsorption and (c, d) SEM images after MnCe/MIL-100 adsorbs TC solution.

Table 1
Element content of MnCe/MIL-100 adsorbent before and after TC adsorption

Elements	Weight %	Atomic %	After adsorption weight %	After adsorption atomic %
C K	0.60	18.77	0.76	22.85
N K	0.06	1.62	0.11	2.08
O K	2.48	58.61	2.55	60.32
Mn K	0.14	0.97	0.08	0.68
Fe K	2.05	13.90	1.62	10.84
Ce L	2.27	6.13	1.76	3.23
Total	7.60	1	6.88	1
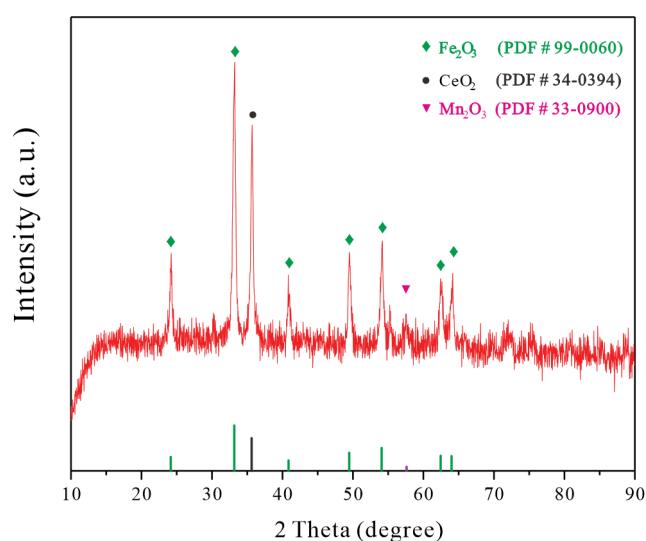
Fig. 2. XRD pattern of MnCe/MIL-100.

Fig. 3. Effect of MnCe/MIL-100 dosage on TC removal efficiency and adsorption capacity. Reaction conditions: $[TC]_0$ = 10 mg/L; volume = 100 mL; time = 18 h.

(024), (116), (214) and (300) crystal planes of Fe_2O_3 (PDF # 99-0060), respectively. In 2θ The diffraction peak at 35.63° corresponds to the characteristic diffraction peak of Mn_2O_3 (PDF # 33-0900), and the diffraction peak at 2θ The diffraction peak at 57.51° corresponds to the characteristic diffraction peak of CeO_2 (PDF # 34-0394) [30], which indicates that a small amount of Mn and Ce oxides are generated. Obviously, MnCe/MIL-100 adsorbent has been successfully prepared, and its diffraction peak is high and sharp, indicating that the adsorbent has good crystallinity.

3.2. Effect of adsorbent dosage on adsorption performance

As shown in Fig. 3, the effects of 5, 10, 15, 20, 25 and 30 mg MnCe/MIL-100 on TC adsorption capacity were investigated. It can be seen from the figure that when the amount of adsorbent added is increased from 5 mg to 30 mg, the TC removal rate increases from 54.83% to 100%. When the amount of MnCe/MIL-100 is 15 mg, the adsorption capacity reaches 66.02 mg/g. Then, when the adsorbent is continuously added to the solution, the removal of TC by MnCe/MIL-100 reaches saturation and TC is completely removed. This is because the active site of MnCe/MIL-100 is in direct proportion to its dosage, and with the increase of dosage, the number of surface active sites increases, and

the adsorption of TC is also improved. However, when the amount of adsorbent added reaches a certain level, the absorption amount of adsorbent will tend to be saturated, so that the adsorption amount of adsorbent in TC solution will be reduced. At this time, the continuous addition of adsorbent to TC solution will not improve the adsorption capacity. To sum up, considering the corresponding economic cost, the dosage of 15 mg was selected for the adsorption experiment and related discussion under the same experimental conditions.

3.3. Effect of initial pH of TC solution on adsorption performance

The influence of zeta potential of adsorbent and pH of aqueous solution on TC adsorption and the exploration of adsorption mechanism are very important [31]. TC molecules have three water dissociation constants (pKα = 3.3, 7.68, 9.69), depending on the pH value. Therefore, TC exists in the form of cations (TC^+), zwitterions (TC^0) and anions (TC^-, TC^{2-}) [32,33]. Therefore, the experiment was set in the range of pH = 3–12 to investigate the effect of MnCe/MIL-100 on TC adsorption. The results are shown in Fig. 4, it can be seen from the figure that when the pH of TC solution is increased from 3 to 9, the removal rate of MnCe/MIL-100 for TC is basically consistent, and the removal rate is

as high as 89.57% at pH 6. This may be because when the pH is strongly acidic, too much H^+ will cause the protonation of MnCe/MIL-100, and finally weaken the electrostatic interaction during TC adsorption. When 4 < pH < 9, TC molecules mainly exist in the form of zwitterions and anions, and TC molecules are electrostatically attracted by the positively charged MnCe/MIL-100 adsorbent [34]. As shown in zeta potential Fig. 5, the pH_{pzc} of MnCe/MIL-100 is 9.44. When pH > 9, the surface of MnCe/MIL-100 is negatively charged. At this time, TC molecules and adsorbent are negatively charged, and electrostatic repulsion occurs between them, resulting in a reduction in the removal rate of TC by MnCe/MIL-100 [33]. This is consistent with the fitting results of adsorption kinetics.
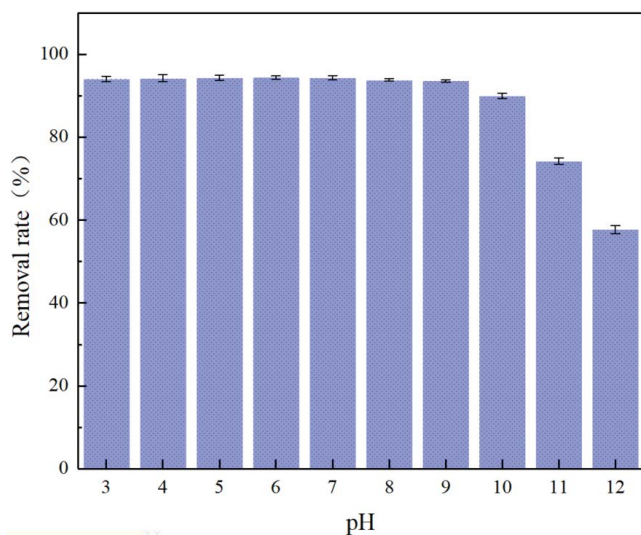
Fig. 4. Effect of pH on removal of TC by MnCe/MIL-100 adsorbent. Reaction conditions: $[MnCe/MIL-100]_0$ = 15 mg; $[TC]_0$ = 10 mg/L; volume = 100 mL; time = 20 h.
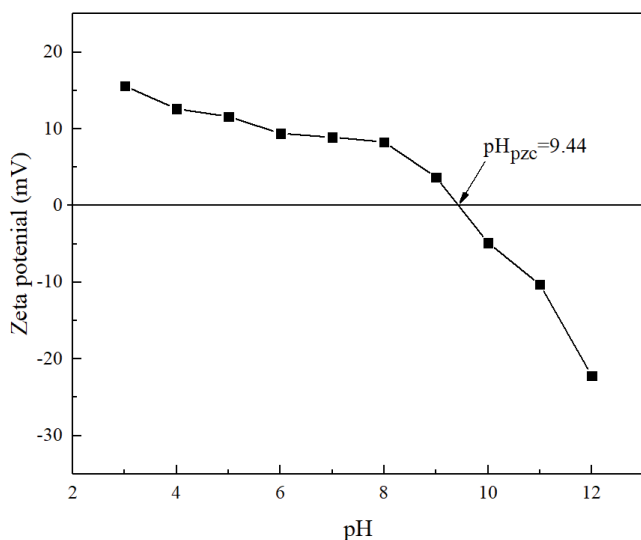
Fig. 5. Zeta potential of MnCe/MIL-100 adsorbent.

3.4. Study on adsorption isotherm

In order to study the interaction process between the adsorbent and the adsorbent and the equilibrium performance of the adsorbent and explore the reaction mechanism of the adsorbent for TC adsorption reaction, two adsorption isotherm models, Langmuir model and Freundlich model, were used to describe the interaction process between the adsorbent molecules and the adsorbent surface and calculate the maximum adsorption capacity [35,36]. Langmuir isotherm equation assumes that the adsorption layer is homogeneous adsorption of single molecule, and each molecule has adsorption activation energy and isoenthalpy. The Freundlich adsorption isotherm equation can be applied to multi-layer adsorption, which is a reversible non ideal and non-uniform adsorption process [37,38]. The expressions of the two models are:

$$\frac{C_e}{q_e} = \frac{C_e}{q_m} + \frac{1}{K_1 + q_m} \tag{3}$$

$$\ln q_e = \frac{1}{n}\ln C_e + \ln K_F \tag{4}$$

where C_e (mg/L) is the concentration after equilibrium adsorption; q_e (mg/g) is the adsorption capacity after equilibrium, and q_m (mg/g) is the maximum adsorption capacity calculated according to Langmuir equation; K_l (L/mg) is the adsorption constant of Langmuir equation; k_F (mg/g), n is the adsorption constant of Freundlich equation.

Fig. 6a–c describe the fitting of the adsorption isotherm model to the experimental data at 298, 308 and 318 K. The parameters of the corresponding isotherm model are listed in Table 2. It can be seen from the figure that the adsorption effect of MnCe/MIL-100 on TC increases with the increase of temperature. The correlation coefficient indicates that the R^2 obtained from the Langmuir model is obviously higher than that of the Freundlich, so the Langmuir model can better fit the adsorption process of MnCe/MIL-100 on TC. At the same time, K_l is in the range of 0–1, which indicates that the adsorption process is favorable and the adsorption of MnCe/MIL-100 adsorbent on TC belongs to uniform monolayer adsorption, and the surface active sites of MnCe/MIL-100 are evenly distributed [24,39]. When TC is attached to the adsorption sites on the surface of MnCe/MIL-100, this adsorption site stops adsorption and the adsorption capacity of the adsorbent reaches a maximum of when TC completely occupies the adsorption site on the adsorbent surface [23]. According to the calculation of Langmuir isotherm model, the maximum adsorption capacity of TC at 298, 308 and 318 K is 210.971, 241.546 and 262.467 mg/g, respectively, which indicates that increasing the temperature is beneficial to the adsorption. In addition, in order to reflect the advantages of MnCe/MIL-100 adsorbent, Table 3 lists the comparison of adsorption capacity with other adsorbents. It can be seen from the table that MnCe/MIL-100 has a higher adsorption capacity than other adsorbents at the same temperature, the optimal pH is neutral, and with a wider pH adaptation range, so there is no need to add acids and bases, thus saving cost.
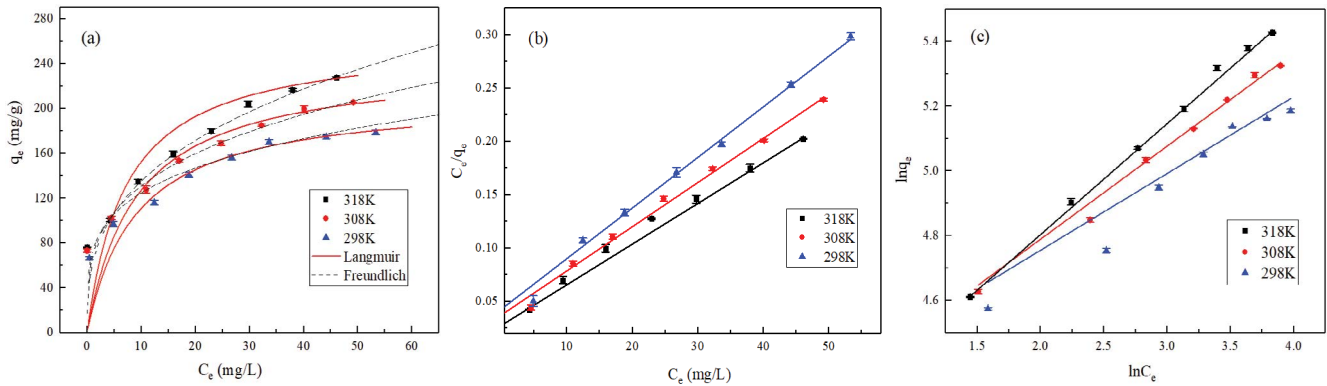
Fig. 6. (a) Isotherm of MnCe/MIL-100 adsorbing TC and (b, c) are linear fitting curves of Langmuir model and Freundlich model of MnCe/MIL-100 adsorbing TC, respectively. Reaction conditions: [MnCe/MIL-100]$_0$ = 15 mg; volume = 100 mL; time = 18 h.

Table 2
Parameters of isotherm model of MnCe/MIL-100 adsorbing TC

Model	Langmuir			Freundlich		
T (K)	K_L	q_m (mg/g)	R^2	n	k_F	R^2
298	0.111	210.971	0.994	2.915	61.375	0.991
308	0.111	241.546	0.993	3.484	67.559	0.987
318	0.138	262.467	0.996	4.219	72.240	0.862

3.5. Kinetic study

In order to further understand the relationship between the structure of the adsorbent and the adsorption form, the adsorption rate and adsorption efficiency of the adsorbent to the adsorbate molecules are described by using two pseudo-first-order and pseudo-second-order kinetic models to explore the adsorption kinetics of the whole adsorption process [45]. The linear forms of the two models are:

$$\ln\left(q_e - q_t\right) = \ln q_e - \frac{k_1 t}{2.303} \tag{5}$$

$$\frac{t}{q_e} = \frac{1}{k_e q_e^2} + \frac{t}{q_e} \tag{6}$$

where q_e and q_t (mg/g) are the amount of TC adsorbed at equilibrium and at a certain time respectively; t (min) is the adsorption time; k_1 (min^{-1}) and k_2 (g/mg·min) are the rate constants of pseudo-first-order and pseudo-second-order reactions, respectively.

Fig. 7a–c show the kinetic model fitting the adsorption process of MnCe/MIL-100 for TC in a certain time. It can be seen from the figure that in the first 300 min, the adsorption speed is fast, while in the period of 300–1,080 min, the adsorption rate starts to slow down, and after 1,080 min, it reaches equilibrium. The possible reason is that there are many active sites that have not been adsorbed at the beginning of the reaction, and TC can quickly bind to the active sites through rapid diffusion on the surface of MnCe/MIL-100 in solution. With the progress of the reaction, the

Table 3
Comparison of adsorption capacity of different adsorbents

Adsorbents	T (K)	pH	TC (mg/L)	q_{max} (mg/g)	Reference
Cu-immobilized alginate	318	3	90	53.26	[40]
La-modified magnetic composite	298	7	25	145.9	[41]
Fe$_3$O$_4$@PDA-SO$_3$H	298	4	20	138.98	[42]
Zr/Cht/Pt	298	4	25	104.166	[43]
HKUST-1	298	6	30	136.88	[44]
MnCe/MIL-100	298	7	10	210.971	Present work
	308			241.546	
	318			262.467	

active sites are occupied continuously, which slows down the adsorption rate and tends to saturation. From the fitting of kinetic parameters in Table 4, it can be seen that the R^2 = 0.999 fitted by the pseudo-second-order kinetic model is greater than the R^2 = 0.996 fitted by the pseudo-first-order kinetic model. Therefore, the pseudo-second-order kinetic model can better describe the adsorption process of MnCe/MIL-100 on TC, and it can be judged that the adsorption process of MnCe/MIL-100 on TC is dominated by chemical adsorption [46,47], and there is strong electrostatic interaction between the adsorbent and TC [48], electronic exchange or sharing occurs between materials and surface groups [49].

3.6. Study on adsorption thermodynamics

In order to explore the influence of temperature on the adsorption process, the adsorption thermodynamic model was used to simulate the parameter change of intrinsic energy in the adsorption reaction process, and Gibbs free energy change (ΔG), enthalpy change (ΔH) and entropy change (ΔS) etc. to explore the spontaneity and randomness of adsorption reaction [50,51]. The thermodynamic calculation formula is as follows [52–54]:
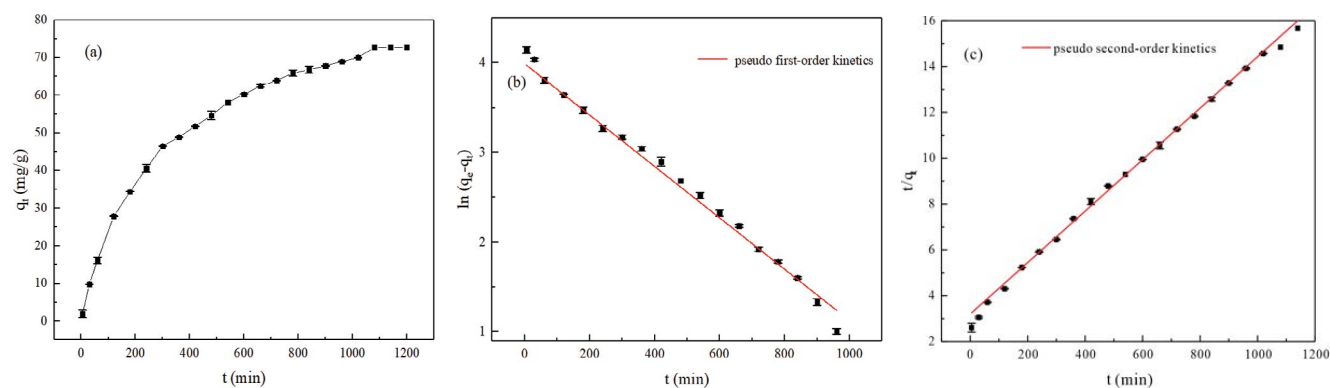
Fig. 7. (a) Kinetic experimental data diagram of MnCe/MIL-100 adsorbing TC, (b) pseudo-first-order kinetic curve, and (c) pseudo-second-order kinetic curve. Reaction conditions: [MnCe/MIL-100]$_0$ = 15 mg; [TC]$_0$ = 10 mg/L; volume = 100 mL; time = 18 h.

Table 4
Pseudo-first-order and pseudo-second-order kinetic fitting parameters of MnCe/MIL-100 adsorbing TC

Pseudo-first-order kinetic			Pseudo-second-order kinetic		
k_1 (min^{-1})	q_e (mg/g)	R^2	k_2 (g/mg·min)	q_e (mg/g)	R^2
0.007	54.055	0.996	0.039×10^{-3}	89.286	0.999

Table 5
Thermodynamic parameters of MnCe/MIL-100 adsorbing TC

Sample	T (K)	ΔG (kJ/mol)	ΔS (kJ/K·mol)	ΔH (kJ/mol)
MnCe/MIL-100	298	−3.080		
	308	−4.313	0.127	34.871
	318	−5.627		

$$\Delta G = -RT \ln K_d \tag{7}$$

$$K_d = M_W \times 55.5 \times 1000 \times K_L \tag{8}$$

$$\ln K_d = -\frac{\Delta H}{RT} + \frac{\Delta S}{R} \tag{9}$$

where R is the general gas constant (8.314 J/(mol·k)); T (K) is the absolute temperature; K_d is denoted thermodynamic equilibrium constant (dimensionless); ΔG is the Gibbs free energy change; ΔH is enthalpy change; ΔS is the entropy change; 55.5 is the number of moles of pure water per liter (1,000 g/L divided by 18 g/mol), and K_l (L/mg) is the Langmuir adsorption equilibrium constant, the molecular weight of the adsorbate (TC) (Mw; g/mol).

The thermodynamic results are shown in Table 5. At 298, 308 and 318 K, the ΔG value is negative, which indicates that the adsorption of TC on MnCe/MIL-100 is a spontaneous process. When the temperature increases from 298 to 318 K, the value of ΔG decreases from −3.080 to −5.627 kJ/mol this negative growth trend confirms that the adsorption reaction is more favorable at a relatively high temperature, and the adsorption reaction is more spontaneous and feasible [55,56]. The value of ΔH in this experiment is 34.871 kJ/mol, which indicates that certain chemical actions are involved in the whole adsorption process. In addition, $\Delta H > 0$ indicates the typical endothermic property of the adsorption process. At the same time $\Delta S > 0$, it means that the chaos and randomness at the interface between adsorbent and adsorbent increase, and the reaction is irreversible, which is conducive to the

stability of adsorption [57]. In conclusion, increasing the temperature will be conducive to the adsorption reaction.

3.7. Effect of recycling of MnCe/MIL-100 on adsorption

Recoverability is an important indicator to evaluate the adsorption performance and application significance of adsorbent, and successful recycling is an important way to improve the efficiency of adsorbent [58]. In this study, a certain amount of saturated adsorbent was put into 0.1 mol/L NaOH solution for desorption for 5 h and dried. Under the same experimental conditions, five cycle regeneration experiments were repeated. In this experiment, considering that MnCe/MIL-100 adsorbent has a low removal rate of TC in the environment with high pH, and that both MnCe/MIL-100 adsorbent and TC have negative charges and certain electrostatic repulsion under strong alkaline conditions, weak alkaline NaOH solution is selected as the eluent [59]. The experimental results are shown in Fig. 8. The removal rate decreases to a certain extent after each cycle of the experiment. This is because TC molecules fill the pore structure in MnCe/MIL-100 adsorbent, thus occupying the adsorption active sites and reducing the active sites. This is an irreversible process [60]. However, after five times of cyclic adsorption, the adsorption and removal efficiency can still remain above 81%. The experimental results show that MnCe/MIL-100 adsorbent has good adsorption and regeneration effect on TC, and has certain reusability.

3.8. Adsorption mechanism

The functional group of the adsorbent is one of the important factors affecting the adsorption efficiency. FT-IR
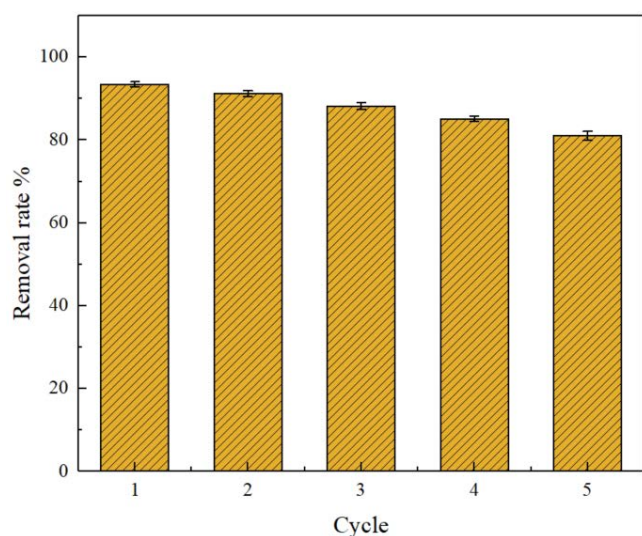
Fig. 8. Regeneration performance of MnCe/MIL-100 adsorbent. Reaction conditions: $[MnCe/MIL-100]_0$ = 15 mg; $[TC]_0$ = 10 mg/L; volume = 100 mL; time = 20 h.
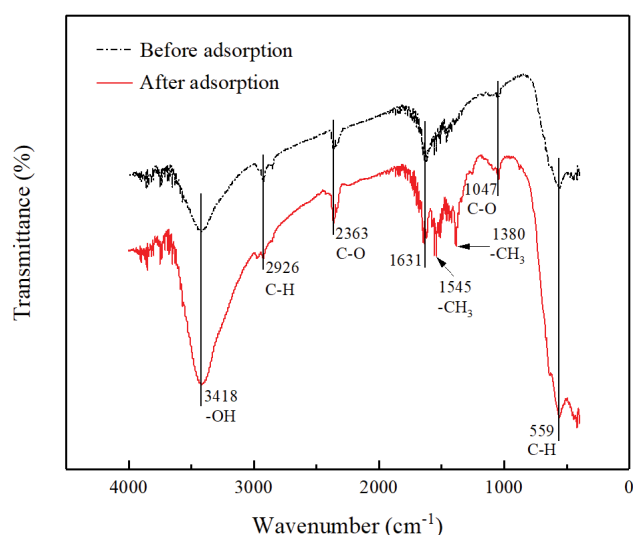
Fig. 9. FT-IR of MnCe/MIL-100 adsorbent.

spectrum is used to identify the functional group of the adsorbent before and after TC adsorption and the changes of atomic and molecular vibration. As shown in Fig. 9, the peak at 3,418 cm^{-1} belongs to the stretching vibration of –OH from the adsorbed water on the adsorbent surface [61], while the peak at 2,926 cm^{-1} is caused by the antisymmetry stretching vibration of C–H of aliphatic. The peak at 2,363 cm^{-1} can be attributed to the stretching vibration of the C–O bond. The peak at 1,631 cm^{-1} can be attributed to the deformation of water molecules, indicating the presence of adsorbed water on the material [21,62]. The peak at 1,047 cm^{-1} is caused by C–O vibration [63]. A C–H vibration peak appears at 559 cm^{-1} [64]. However, new characteristic peaks appeared at 1,545 and 1,380 cm^{-1} after TC adsorption, which is due to the stretching vibration of aromatic ring group and the bending vibration of –CH$_3$ of TC, and

the skeleton vibration absorption peaks of the benzene ring in the tetracycline molecule after TC adsorption [65], this indicates that C–H group in the material forms hydrogen bond with phenol hydroxyl group on the surface of TC [66]. This further proves that TC is adsorbed on MnCe/MIL-100.

The adsorption isotherm, kinetic and thermodynamic results showed that the adsorption of TC by MnCe/MIL-100 was spontaneous, endothermic and homogeneous. In addition, the adsorption between MnCe/MIL-100 and TC is realized by sharing electrons and forming chemical bonds between functional groups. The high specific surface area and good conductivity of MnCe/MIL-100 provide more adsorption sites for TC adsorption. zeta potential results show that the electrostatic interaction between positively charged MnCe/MIL-100 and zwitter-ionic TC is an important reason for their adsorption.

4. Conclusion

In this study, MnCe/MIL-100 adsorbent was prepared by simple solvothermal method, which has good adsorption performance for TC. The results of adsorption kinetics and isotherm show that the adsorption process conforms to the pseudo-second-order kinetics and Langmuir model, and it can be judged that the adsorption of TC by MnCe/MIL-100 is dominated by chemical adsorption and belongs to uniform monolayer adsorption. The adsorption thermodynamic results showed that the adsorption capacity of the adsorbent for TC increased with the increase of temperature. The thermodynamic parameters $\Delta G < 0$, and both ΔH and ΔS are greater than 0, indicating that the adsorption is endothermic and spontaneous. The results of solution pH influence show that the adsorption performance starts to decrease at higher pH environment, which may be due to the negative charge on the surface of MnCe/MIL-100 and the negative charge on the TC molecule at this time. Electrostatic repulsion occurs between the two, resulting in the reduction of the adsorption effect of MnCe/MIL-100 on TC. In addition, MnCe/MIL-100 adsorbent can still maintain high TC removal efficiency after repeated regeneration with NaOH, and has good reusability, indicating that it has practical application potential.

References

[1] M. Nie, Y. Li, J. He, C. Xie, Z. Wu, B. Sun, K. Zhang, L. Kong, J. Liu, Degradation of tetracycline in water using Fe$_3$O$_4$ nanospheres as Fenton-like catalysts: kinetics, mechanisms and pathways, New J. Chem., 44 (2020) 2847–2857.

[2] K. Sun, F. Cheng, Y. Liu, Y. Hua, Y. Zhang, Microwave-assisted iron oxide process for efficient removal of tetracycline, J. Environ. Manage., 307 (2022) 114600, doi: 10.1016/j.jenvman.2022.114600.

[3] X. Wang, J. Jia, Y. Wang, Combination of photocatalysis with hydrodynamic cavitation for degradation of tetracycline, Chem. Eng. J., 315 (2017) 274–282.

[4] A.M. Voigt, H.A. Faerber, G. Wilbring, D. Skutlarek, C. Felder, R. Mahn, D. Wolf, P. Brossart, T. Hornung, S. Engelhart, M. Exner, R.M. Schmithausen, The occurrence of antimicrobial substances in toilet, sink and shower drainpipes of clinical units: a neglected source of antibiotic residues, Int. J. Hyg. Environ. Health, 222 (2019) 455–467.

[5] K. Wang, T. Zhuang, Z. Su, M. Chi, H. Wang, Antibiotic residues in wastewaters from sewage treatment plants and pharmaceutical industries: occurrence, removal and environmental impacts, Sci. Total Environ., 788 (2021) 147811, doi: 10.1016/j.scitotenv.2021.147811.

[6] L. Tong, L. Qin, C. Xie, H. Liu, Y. Wang, C. Guan, S. Huang, Distribution of antibiotics in alluvial sediment near animal breeding areas at the Jianghan Plain, Central China, Chemosphere, 186 (2017) 100–107.

[7] D. Zhang, K.Zhang, X. Hu, Y. Xue, L. Zhang, Y. Sun, Ball-milled biochar incorporated polydopamine thin-film composite (PDA/TFC) membrane for high-flux separation of tetracyclic antibiotics from wastewater, Sep. Purif. Technol., 272 (2021) 118957, doi: 10.1016/j.seppur.2021.118957.

[8] J. Huang, P. Xue, S. Wang, S. Han, L. Lin, X. Chen, Z. Wang, Fabrication of zirconium-based metal-organic frameworks@ tungsten trioxide (UiO-66-NH$_2$@WO$_3$) heterostructure on carbon cloth for efficient photocatalytic removal of tetracycline antibiotic under visible light, J. Colloid Interface Sci., 606 (2022) 1509–1523.

[9] R. Sun, J. Yang, R. Huang, C. Wang, Controlled carbonization of microplastics loaded nano zero-valent iron for catalytic degradation of tetracycline, Chemosphere, 303 (2022) 135123, doi: 10.1016/j.chemosphere.2022.135123.

[10] C. Wang, R. Sun, R. Huang, H. Wang, Superior Fenton-like degradation of tetracycline by iron loaded graphitic carbon derived from microplastics: synthesis, catalytic performance, and mechanism, Sep. Purif. Technol., 270 (2021) 118773, doi: 10.1016/j.seppur.2021.118773.

[11] Z. He, X. Wang, Y. Luo, Y. Zhu, X. Lai, J. Shang, J. Chen, Q. Liao, Effects of suspended particulate matter from natural lakes in conjunction with coagulation to tetracycline removal from water, Chemosphere, 277 (2021) 130327, doi: 10.1016/j.chemosphere.2021.130327.

[12] Z. Zhao, G. Zhang, Y. Zhang, M. Dou, Y. Li, Fe$_3$O$_4$ accelerates tetracycline degradation during anaerobic digestion: synergistic role of adsorption and microbial metabolism, Water Res., 185 (2020) 116225, doi: 10.1016/j.watres.2020.116225.

[13] S. Ranjbari, B. Tanhaei, A. Ayati, S. Khadempir, M. Sillanpaa, Efficient tetracycline adsorptive removal using tricapryl-methylammonium chloride conjugated chitosan hydrogel beads: mechanism, kinetic, isotherms and thermodynamic study, Int. J. Biol. Macromol., 155 (2020) 421–429.

[14] J. Liu, H. Lin, Y. Dong, Y. He, W. Liu, Y. Shi, The effective adsorption of tetracycline onto MoS$_2$@Zeolite-5: adsorption behavior and interfacial mechanism, J. Environ. Chem. Eng., 9 (2021) 105912, doi: 10.1016/j.jece.2021.105912.

[15] J. Tao, J. Yang, C. Ma, J. Li, K. Du, Z. Wei, C. Chen, Z. Wang, C. Zhao, X. Deng, Cellulose nanocrystals/graphene oxide composite for the adsorption and removal of levofloxacin hydrochloride antibiotic from aqueous solution, R. Soc. Open Sci., 7 (2020) 200857, doi: 10.1098/rsos.200857.

[16] Z. Song, Y.L. Ma, C.E. Li, The residual tetracycline in pharmaceutical wastewater was effectively removed by using MnO$_2$/graphene nanocomposite, Sci. Total Environ., 651 (2019) 580–590.

[17] D. Hao, Y. Chen, Y. Zhang, N. You, Nanocomposites of zero-valent iron@biochar derived from agricultural wastes for adsorptive removal of tetracyclines, Chemosphere, 284 (2021) 131342, doi: 10.1016/j.chemosphere.2021.131342.

[18] H. Qiao, X. Wang, P. Liao, C. Zhang, C. Liu, Enhanced sequestration of tetracycline by Mn(II) encapsulated mesoporous silica nanoparticles: synergistic sorption and mechanism, Chemosphere, 284 (2021) 131334, doi: 10.1016/j.chemosphere.2021.131334.

[19] Z. Qiu, Q. Lin, J. Lin, X. Zhang, Y. Wang, Regenerable Mg/Fe bimetallic hydroxide for remarkable removal of low-concentration norfloxacin from aqueous solution, Colloids Surf., A, 644 (2022) 128825, doi: 10.1016/j.colsurfa.2022.128825.

[20] J. Yu, H. Wang, Q. Ji, Investigating adsorption mechanism and surface complex formation modeling for aqueous sulfadiazine bonding on Fe/Mn binary oxides, Environ. Sci. Pollut. Res. Int., 26 (2019) 23162–23172.

[21] K. Wu, C. Zhang, T. Liu, H. Lei, S. Yang, P. Jin, The removal of tetracycline, oxytetracycline, and chlortetracycline by manganese oxide-doped copper oxide: the behaviors and insights of Cu-Mn combination for enhancing antibiotics removal, Environ. Sci. Pollut. Res., 27 (2020) 12613–12623.

[22] L. Wang, D. Luo, J. Yang, C. Wang, Metal-organic frameworks-derived catalysts for contaminant degradation in persulfate-based advanced oxidation processes, J. Cleaner Prod., 375 (2022) 134118, doi: 10.1016/j.jclepro.2022.134118.

[23] X. Ma, W. Wang, C. Sun, H. Li, J. Sun, X. Liu, Adsorption performance and kinetic study of hierarchical porous Fe-based MOFs for toluene removal, Sci. Total Environ., 793 (2021) 148622, doi: 10.1016/j.scitotenv.2021.148622.

[24] W. Li, T. Zhang, L. Lv, Y. Chen, W. Tang, S. Tang, Room-temperature synthesis of MIL-100(Fe) and its adsorption performance for fluoride removal from water, Colloids Surf., A, 624 (2021) 126791, doi: 10.1016/j.colsurfa.2021.126791.

[25] C. Liang, X. Zhang, P. Feng, H. Chai, Y. Huang, ZIF-67 derived hollow cobalt sulfide as superior adsorbent for effective adsorption removal of ciprofloxacin antibiotics, Chem. Eng. J., 344 (2018) 95–104.

[26] A.S. Eltaweil, H.M. Elshishini, Z.F. Ghatass, G.M. Elsubruiti, Ultra-high adsorption capacity and selective removal of Congo red over aminated graphene oxide modified Mn-doped UiO-66 MOF, Powder Technol., 379 (2021) 407–416.

[27] I. Bezverkhyy, E. Popova, N. Geoffroy, F. Herbst, J. Bellat, Preparation of magnetic composites of MIL-53(Fe) or MIL-100(Fe) via partial transformation of their framework into γ-Fe$_2$O$_3$, J. Mater. Chem. A, 4 (2016) 8141–8148.

[28] Y. Guo, C. Yan, P. Wang, L. Rao, C. Wang, Doping of carbon into boron nitride to get the increased adsorption ability for tetracycline from water by changing the pH of solution, Chem. Eng. J., 387 (2020) 124136, doi: 10.1016/j.cej.2020.124136.

[29] B. Sun, Y.M. Cheng, F.W. Xu, F. Liu, J. Zhang, Z. Tang, Y. Wang, J.Y. Liu, S.G. Zhu, X.L. Cai, Study on the adsorption performance of Ni-Mo-S nanomaterials for Congo red in azo wastewater, Desal. Water Treat., 234 (2021) 267–276.

[30] J. Ouyang, Z. Zhao, S. Suib, H. Yang, Degradation of Congo red dye by a Fe$_2$O$_3$@CeO$_2$-ZrO$_2$/Palygorskite composite catalyst: synergetic effects of Fe$_2$O$_3$, J. Colloid Interface Sci., 539 (2019) 135–145.

[31] K.A. Lin, Y.T. Liu, S.Y. Chen, Adsorption of fluoride to UiO-66-NH$_2$ in water: stability, kinetic, isotherm and thermodynamic studies, J. Colloid Interface Sci., 461 (2016) 79–87.

[32] J. Xia, Y. Gao, G. Yu, Tetracycline removal from aqueous solution using zirconium-based metal-organic frameworks (Zr-MOFs) with different pore size and topology: adsorption isotherm, kinetic and mechanism studies, J. Colloid Interface Sci., 590 (2021) 495–505.

[33] J. Kang, H. Liu, Y.M. Zheng, J. Qu, J.P. Chen, Application of nuclear magnetic resonance spectroscopy, Fourier transform infrared spectroscopy, UV-Visible spectroscopy and kinetic modeling for elucidation of adsorption chemistry in uptake of tetracycline by zeolite beta, J. Colloid Interface Sci., 354 (2011) 261–267.

[34] B.V. Chang, F.Y. Hsu, H.Y. Liao, Biodegradation of three tetracyclines in swine wastewater, J. Environ. Sci. Health., Part B, 49 (2014) 449–455.

[35] Z. Mengting, T.A. Kurniawan, R. Avtar, M.H.D. Othman, T. Ouyang, H. Yujia, Z. Xueting, T. Setiadi, I. Iswanto,

Applicability of TiO$_2$(B) nanosheets@hydrochar composites for adsorption of tetracycline (TC) from contaminated water, J. Hazard. Mater., 405 (2021) 123999, doi: 10.1016/j.jhazmat.2020.123999.

[36] X.F. Yan, X.R. Fan, Q. Wang, Y. Shen, An adsorption isotherm model for adsorption performance of silver-loaded activated carbon, Therm. Sci., 21 (2017) 1645–1649.

[37] M.A. Al-Ghouti, D.A. Da'ana, Guidelines for the use and interpretation of adsorption isotherm models: a review, J. Hazard. Mater., 393 (2020) 122383, doi: 10.1016/j.jhazmat.2020.122383.

[38] L.P. Lingamdinne, J. Choi, G.K.R. Angaru, R.R.K., J. Yang, Y. Chang, J.R. Koduru, Magnetic-watermelon rinds biochar for uranium-contaminated water treatment using an electromagnetic semi-batch column with removal mechanistic investigations, Chemosphere, 286 (2022) 131776, doi: 10.1016/j.chemosphere.2021.131776.

[39] X. Zhang, Y. Yang, L. Song, J. Chen, Y. Yang, Y. Wang, Enhanced adsorption performance of gaseous toluene on defective UiO-66 metal organic framework: equilibrium and kinetic studies, J. Hazard. Mater., 365 (2019) 597–605.

[40] X. Zhang, X. Lin, Y. He, Y. Chen, X. Luo, R. Shang, Study on adsorption of tetracycline by Cu-immobilized alginate adsorbent from water environment, Int. J. Biol. Macromol., 124 (2019) 418–428.

[41] X. Mi, X. Wang, F. Zhou, X. Chai, W. Wang, F. Zhang, S. Meng, Y. Shang, W. Zhao, G. Li, Preparation of La-modified magnetic composite for enhanced adsorptive removal of tetracycline, Environ. Sci. Pollut. Res., 24 (2017) 17127–17135.

[42] Y. Li, X. Lin, C. Zhang, Q. Zhuang, W. Dong, Polydopamine magnetic microspheres grafted with sulfonic acid groups for efficient adsorption of tetracycline, Colloids Surf., A, 628 (2021) 127263, doi: 10.1016/j.colsurfa.2021.127263.

[43] B. Turan, G. Sarigol, P. Demircivi, Adsorption of tetracycline antibiotics using metal and clay embedded cross-linked chitosan, Mater. Chem. Phys., 279 (2022) 125781, doi: 10.1016/j.matchemphys.2022.125781.

[44] J. Pan, X. Bai, Y. Li, B. Yang, P. Yang, F. Yu, J. Ma, HKUST-1 derived carbon adsorbents for tetracycline removal with excellent adsorption performance, Environ. Res., 205 (2022) 112425, doi: 10.1016/j.envres.2021.112425.

[45] B. Debnath, M. Majumdar, M. Bhowmik, K.L. Bhowmik, A. Debnath, D.N. Roy, The effective adsorption of tetracycline onto zirconia nanoparticles synthesized by novel microbial green technology, J. Environ. Manage., 261 (2020) 110235, doi: 10.1016/j.jenvman.2020.110235.

[46] X. Fang, S. Wu, Y. Wu, W. Yang, Y. Li, J. He, P. Hong, M. Nie, C. Xie, Z. Wu, K. Zhang, L. Kong, J. Liu, High-efficiency adsorption of norfloxacin using octahedral UIO-66-NH$_2$ nanomaterials: dynamics, thermodynamics, and mechanisms, Appl. Surf. Sci., 518 (2020) 146226, doi: 10.1016/j.apsusc.2020.146226.

[47] A. Lim, J.J. Chew, L.H. Ngu, S. Ismadji, D.S. Khaerudini, J. Sunarso, Synthesis, characterization, adsorption isotherm, and kinetic study of oil palm trunk-derived activated carbon for tannin removal from aqueous solution, ACS Omega, 5 (2020) 28673–28683.

[48] B. Sun, J. Zhang, C. Ding, F. Xu, Y. Cheng, Z. Tang, F. Pan, J. Liu, S. Zhu, Synthesis and characterization of Fe-Al-Ni ternary composite metal oxides as highly efficient adsorbent for fluoride removal from water, Desal. Water Treat., 229 (2021) 243–251.

[49] C. Wang, H. Wang, Y. Cao, Pb(II) sorption by biochar derived from *Cinnamomum camphora* and its improvement with ultrasound-assisted alkali activation, Colloids Surf., A, 556 (2018) 177–184.

[50] M. Tuzen, A. Sari, T.A. Saleh, Response surface optimization, kinetic and thermodynamic studies for effective removal of rhodamine B by magnetic AC/CeO$_2$ nanocomposite, J. Environ. Manage., 206 (2018) 170–177.

[51] S. Li, Y. Guo, M. Xiao, T. Zhang, S. Yao, S. Zang, H. Fan, Y. Shen, Z. Zhang, W. Li, Enhanced arsenate removal from aqueous solution by Mn-doped MgAl-layered double hydroxides, Environ. Sci. Pollut. Res., 26 (2019) 12014–12024.

[52] Y. Li, Z. Wang, X. Xie, J. Zhu, R. Li, T. Qin, Removal of Norfloxacin from aqueous solution by clay-biochar composite prepared from potato stem and natural attapulgite, Colloids Surf., A, 514 (2017) 126–136.

[53] K. Narasimharao, L. Lingamdinne, S. Al-Thabaiti, M. Mokhtar, A. Alsheshri, S. Alfaifi, Y. Chang, J. Koduru, Synthesis and characterization of hexagonal Mg–Fe layered double hydroxide/grapheme oxide nanocomposite for efficient adsorptive removal of cadmium ion from aqueous solutions: isotherm, kinetic, thermodynamic and mechanism, J. Water Process Eng., 47 (2022) 102746, doi: 10.1016/j.jwpe.2022.102746.

[54] Y.X. Song, S. Chen, N. You, H.T. Fan, L.N. Sun, Nanocomposites of zero-valent Iron@Activated carbon derived from corn stalk for adsorptive removal of tetracycline antibiotics, Chemosphere, 255 (2020) 126917, doi: 10.1016/j.chemosphere.2020.126917.

[55] S. Liu, M. Pan, Z. Feng, Y. Qin, Y. Wang, L. Tan, T. Sun, Ultra-high adsorption of tetracycline antibiotics on garlic skin-derived porous biomass carbon with high surface area, New J. Chem., 44 (2020) 1097–1106.

[56] D. Balarak, E. Mostafapour, E. Bazrafshan, T.A. Saleh, Studies on the adsorption of amoxicillin on multi-wall carbon nanotubes, Water Sci. Technol., 75 (2017) 1599–1606.

[57] W. Chen, X. Li, Z. Pan, Y. Bao, S. Ma, L. Li, Efficient adsorption of Norfloxacin by Fe-MCM-41 molecular sieves: kinetic, isotherm and thermodynamic studies, Chem. Eng. J., 281 (2015) 397–403.

[58] C. Lei, M. Pi, C. Jiang, B. Cheng, J. Yu, Synthesis of hierarchical porous zinc oxide (ZnO) microspheres with highly efficient adsorption of Congo red, J. Colloid Interface Sci., 490 (2017) 242–251.

[59] S. Lin, T. Zhang, D. Fu, X. Zhou, Utilization of magnesium resources in salt lake brine and catalytic degradation of dye wastewater by doping cobalt and nickel, Sep. Purif. Technol., 270 (2021) 118808, doi: 10.1016/j.seppur.2021.118808.

[60] Y. Guo, W. Huang, B. Chen, Y. Zhao, D. Liu, Y. Sun, B. Gong, Removal of tetracycline from aqueous solution by MCM-41-zeolite A loaded nano zero valent iron: synthesis, characteristic, adsorption performance and mechanism, J. Hazard. Mater., 339 (2017) 22–32.

[61] T. Liu, K. Wu, W. Xue, C. Ma, Characteristics and mechanisms of arsenate adsorption onto manganese oxide-doped aluminum oxide, Environ. Prog. Sustainable Energy, 34 (2015) 1009–1018.

[62] Y.J.O. Asencios, M.R. Sun-Kou, Synthesis of high-surface-area γ-Al$_2$O$_3$ from aluminum scrap and its use for the adsorption of metals: Pb(II), Cd(II) and Zn(II), Appl. Surf. Sci., 258 (2012) 10002–10011.

[63] D. Xie, H. Zhang, M. Jiang, H. Huang, H. Zhang, Y. Liao, S. Zhao, Adsorptive removal of tetracycline from water using Fe(III)-functionalized carbonized humic acid, Chin. J. Chem. Eng., 28 (2020) 2689–2698.

[64] K. Wang, J. Wu, M. Zhu, Y.Z. Zheng, X. Tao, Highly effective pH-universal removal of tetracycline hydrochloride antibiotics by UiO-66-(COOH)$_2$/GO metal–organic framework composites, J. Solid State Chem., 284 (2020) 121200, doi: 10.1016/j.jssc.2020.121200.

[65] Z. Wang, X. Chen, Z. Meng, M. Zhao, H. Zhan, W. Liu, A water resistance magnetic graphene-anchored zeolitic imidazolate framework for efficient adsorption and removal of residual tetracyclines in wastewater, Water Sci. Technol., 81 (2020) 2322–2336.

[66] Z. Kang, X. Jia, Y. Zhang, X. Kang, M. Ge, D. Liu, C. Wang, Z. He, A review on application of biochar in the removal of pharmaceutical pollutants through adsorption and persulfate-based AOPs, Sustainability, 14 (2022) 10128, doi: 10.3390/su141610128.